RESEARCH ARTICLE

Maturation of the Human Papillomavirus 16 Capsid

Giovanni Cardone,[a] Adam L. Moyer,[b] Naiqian Cheng,[a] Cynthia D. Thompson,[b] Israel Dvoretzky,[c] Douglas R. Lowy,[b] John T. Schiller,[b] Alasdair C. Steven,[a] Christopher B. Buck,[b] Benes L. Trus[d]

Laboratory of Structural Biology, National Institute for Arthritis, Musculoskeletal and Skin Diseases, National Institutes of Health (NIH), Bethesda, Maryland, USA[a]; Laboratory of Cellular Oncology, National Cancer Institute, NIH, Bethesda, Maryland, USA[b]; Yale University, New Haven, Connecticut, USA[c]; Imaging Sciences Laboratory, Center for Information Technology, NIH, Bethesda, Maryland, USA[d]

G.C. and A.L.M. contributed equally to this article.

ABSTRACT **Papillomaviruses are a family of nonenveloped DNA viruses that infect the skin or mucosa of their vertebrate hosts. The viral life cycle is closely tied to the differentiation of infected keratinocytes. Papillomavirus virions are released into the environment through a process known as desquamation, in which keratinocytes lose structural integrity prior to being shed from the surface of the skin. During this process, virions are exposed to an increasingly oxidative environment, leading to their stabilization through the formation of disulfide cross-links between neighboring molecules of the major capsid protein, L1. We used time-lapse cryo-electron microscopy and image analysis to study the maturation of HPV16 capsids assembled in mammalian cells and exposed to an oxidizing environment after cell lysis. Initially, the virion is a loosely connected procapsid that, under *in vitro* conditions, condenses over several hours into the more familiar 60-nm-diameter papillomavirus capsid. In this process, the procapsid shrinks by ~5% in diameter, its pentameric capsomers change in structure (most markedly in the axial region), and the interaction surfaces between adjacent capsomers are consolidated. A C175S mutant that cannot achieve normal inter-L1 disulfide cross-links shows maturation-related shrinkage but does not achieve the fully condensed 60-nm form. Pseudoatomic modeling based on a 9-Å resolution reconstruction of fully mature capsids revealed C-terminal disulfide-stabilized "suspended bridges" that form intercapsomeric cross-links. The data suggest a model in which procapsids exist in a range of dynamic intermediates that can be locked into increasingly mature configurations by disulfide cross-linking, possibly through a Brownian ratchet mechanism.**

IMPORTANCE **Human papillomaviruses (HPVs) cause nearly all cases of cervical cancer, a major fraction of cancers of the penis, vagina/vulva, anus, and tonsils, and genital and nongenital warts. HPV types associated with a high risk of cancer, such as HPV16, are generally transmitted via sexual contact. The nonenveloped virion of HPVs shows a high degree of stability, allowing the virus to persist in an infectious form in environmental fomites. In this study, we used cryo-electron microscopy to elucidate the structure of the HPV16 capsid at different stages of maturation. The fully mature capsid adopts a rigid, highly regular structure stabilized by intermolecular disulfide bonds. The availability of a pseudoatomic model of the fully mature HPV16 virion should help guide understanding of antibody responses elicited by HPV capsid-based vaccines.**

Received 27 March 2014 **Accepted** 7 July 2014 **Published** 5 August 2014

Citation Cardone G, Moyer AL, Cheng N, Thompson CD, Dvoretzky I, Lowy DR, Schiller JT, Steven AC, Buck CB, Trus BL. 2014. Maturation of the human papillomavirus 16 capsid. mBio 5(4):e01104-14. doi:10.1128/mBio.01104-14.

Editor Michael Imperiale, University of Michigan

Address correspondence to Benes L.Trus, trusb@mail.nih.gov.

Papillomaviruses are a diverse group of nonenveloped DNA viruses that replicate exclusively in keratinocytes, a specialized cell type that differentiates to form the protective outer surface of the skin, as well as the oral and genital mucosa. Different papillomavirus species typically infect specific cutaneous or mucosal areas. For example, human papillomavirus 1 (HPV1) often infects the soles of the feet, where it can cause benign skin warts (papillomas) (1). Other HPV types are tropic for the genital mucosa. Although genital HPV infections are generally subclinical and self-limited, women who are persistently infected with any of a dozen or so "high-risk" HPV types can progress to develop HPV-induced cancer of the uterine cervix (2). HPV16 causes a majority of cases of cervical cancer and is also a major cause of cancer of the vagina, vulva, penis, anus, and oropharynx (3).

The papillomavirus life cycle is closely linked to the differentiation program of keratinocytes within stratified squamous epithelial tissues (4). Expression of the viral late genes, such as those encoding the capsid proteins, is restricted to a subset of keratinocytes near the apical surface of the epithelium. The eventual release of virions into the environment depends on desquamation, a differentiation endpoint in which spontaneously disrupted keratinocytes are shed into the environment. Tight coupling of the viral late phase to the normal, noninflammatory process of epithelial differentiation is thought to have evolved as a viral immune evasion mechanism, since it restricts expression of immunogenic viral capsid proteins to superficial layers of the skin, where immune cell surveillance is restricted. A consequence of the differentiation dependency of the late phase of the papillomavirus life

cycle is that the process of virion assembly and release into the environment is very slow, taking days to complete.

The papillomavirus capsid is composed primarily of the major capsid protein, L1, which is necessary and sufficient for formation of a 72-pentamer T=7 icosahedral capsid. If L1 is expressed together with the minor capsid protein, L2, the two proteins can coassemble around chromatinized viral DNA to form infectious virions (5).

We showed previously that papillomavirus capsids assembled within cultured mammalian cells are physically fragile immediately after cell lysis (6). Over the course of many hours, a progressive series of intermolecular disulfide bonds are formed, resulting in a characteristic pattern of two species of L1 dimers and two species of L1 trimers in nonreducing denaturing (SDS-PAGE) gel analyses. Although capsid maturation is not strictly required for infectivity in cell culture, the formation of disulfide bonds physically stabilizes the capsid. Conversely, treatment of the mature capsid with reducing agents or mutation of key cysteine residues within L1 results in a less stable capsid (7–9).

Although capsid maturation is a common feature of many virus types (10), the disulfide dependency and slow kinetics of papillomavirus capsid maturation are unique and may reflect the comparatively languid pace of the late phase of the papillomavirus life cycle *in vivo*. In this study, we used cryo-electron microscopy (cryo-EM) and digital image reconstruction to analyze HPV16 capsids at various stages of this unusual process of maturation.

RESULTS

Purification of immature HPV16 capsids. Papillomavirus capsids are about 60 nm in diameter (11). However, in a cryo-EM study focused on localizing the HPV16 minor capsid protein, L2, we noted the presence of a subset of capsids somewhat larger than 60 nm in diameter (12). This led us to speculate that the larger particles represented capsids that had not completed the process of maturation (6). Since the capsid preparations in the L2 study had been allowed to mature for 18 h and were purified using ultracentrifugation methods designed to enrich for mature capsids, we wondered whether a greater proportion of immature capsid conformations might exist in capsid preparations that were given less time to mature.

Immature HPV16 capsids are known to be physically fragile, and previously described purification methods cause severe distortion, including nucleic acid "evisceration," of immature HPV16 capsids during ultracentrifugal purification (6). Thus, gentler purification methods were needed to produce specimens suitable for examining immature capsid structure by cryo-EM. Agarose gel filtration is a well-established size exclusion chromatography method for purifying large molecules or molecular assemblies (13). We therefore reasoned that agarose gel filtration might be a feasible method for nondisruptive single-step purification of immature capsids from clarified cell lysates.

An initial experiment using capsids allowed to mature for 18 h in cell lysate demonstrated that a single round of agarose gel filtration can produce a capsid preparation with adequate purity and concentration for cryo-EM analysis. However, a subsequent attempt to use agarose gel filtration to purify immature capsids (allowed to mature for only 1 h) resulted in a severe reduction in yield of purified capsids. This reduction in yield correlated with the appearance of precipitated material at the top of the gel filtration column, suggesting that the loss might be due to capsid aggregation and entrapment in the size exclusion resin. Immature papillomavirus capsids are known to be prone to aggregation (14, 15). Furthermore, a paper by Shi and colleagues (16) demonstrated that nonspecific interactions between papillomavirus capsids and solid surfaces can trigger capsid aggregation.

Three procedural modifications were used to improve the yield of immature capsids. A major improvement in yield was achieved by incubating the gel filtration column overnight with 1% bovine serum albumin (BSA). Presumably, this improvement was due to blocking of disruptive nonspecific interactions between the capsids and the resin. Further minor improvements were achieved by performing the gel filtration in phosphate-buffered saline (PBS) with 0.5 M NaCl and/or supplementing the buffer with 0.01% Brij 58, a nonionic detergent (16, 17). When all three measures were employed simultaneously, it was possible to recover at least 50% of the L1 applied to the column as soluble purified capsids. The resulting preparations were adequately concentrated for cryo-EM analysis.

Cryo-EM analysis of mature and immature capsid preparations. Micrographs of gel-filtered capsids that had been allowed to mature for 18 h showed predominantly the familiar 60-nm capsid form (Fig. 1a). However, capsids with larger diameters were also observed (roughly 3 to 5%). Analyzing 7,823 capsid images from 16 micrographs, we were able to obtain three classes of various sizes from 600 Å to 626 Å (Fig. 2), presumably corresponding to the final stages in the maturation of HPV. Although a subpopulation of even larger capsid species was visible in some images, iterative refinement of all images against four size classes of images resulted in two of the classes merging, yielding only 3 classes (as before). This could be due to the limited number of images in the larger size class, or it might simply indicate that the larger classes are too irregular to be accommodated in an icosahedral model.

Next, we incorporated into the analysis gel-filtered capsids that had been allowed to mature for 4 h. Since capsids allowed to mature for 4 h have formed few inter-L1 disulfide bonds (6), we anticipated the appearance of additional, larger classes of capsids more closely resembling the initial immature state. Representative examples of 4-h capsids are illustrated in Fig. 1b.

After combining the 4-h image data, which contained 2,354 images from 16 micrographs, with the 18-h data and analyzing their size distribution with larger capsid models, we found that the shape and size distributions were very similar to the 18-h data (data not shown).

We next incorporated images from a capsid preparation allowed to mature for only 1 h (Fig. 1c). The total data set consisted of 2,801 capsid images from 20 micrographs. The data were refined extensively using multiple size models until convergence, until the output models were similar to the input models. The final result yielded 5 classes with diameters ranging from 600 Å (mature) to 633 Å (less mature). The incorporation of 4-h and 1-h data produced a slightly larger three-dimensional (3D) model (633 Å versus 626 Å). We attribute this difference to the fact that there were too few images of ~633-Å diameter capsids in the 18-h preparation to produce a reasonable 3D reconstruction. The distribution of these datasets is described in Table S1 in the supplemental material. Final results for the 5 models are shown in Fig. 3. The primary benefit of incorporating additional data was obtaining more accurate and better classes due to the presence of more images in the larger size classes. The existence of multiple classes of particles also confirms a previous report showing open and closed

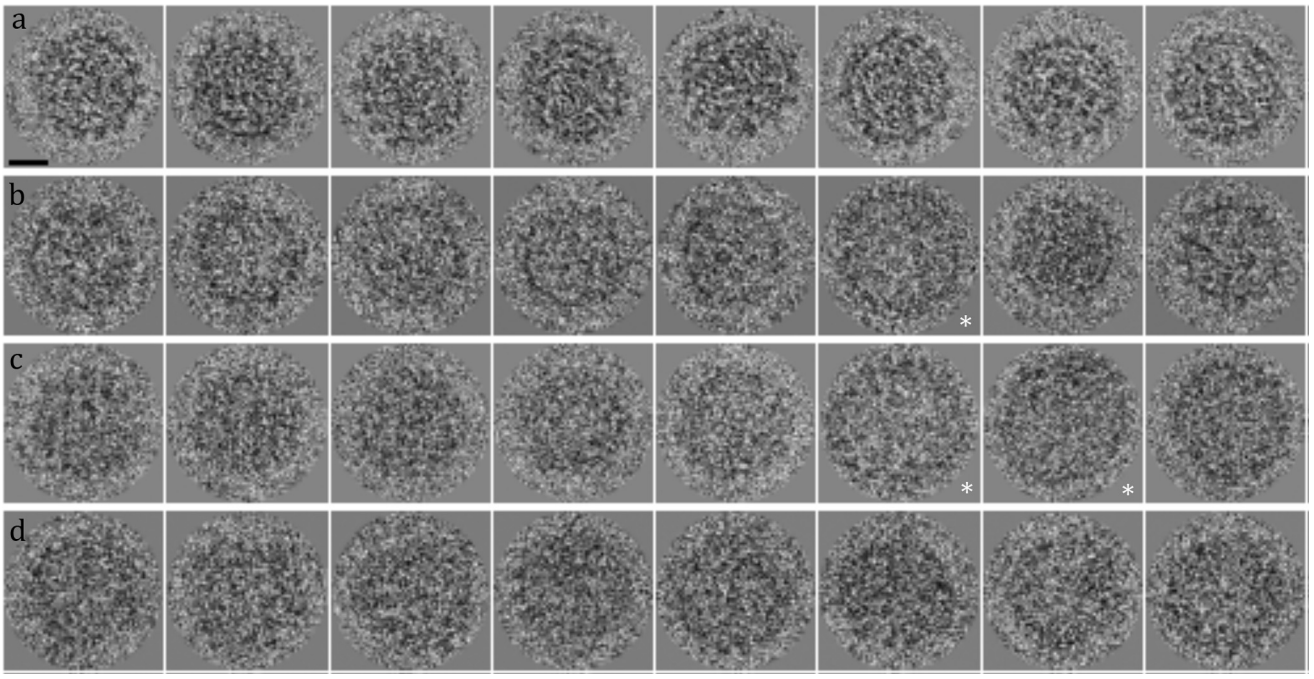

FIG 1 (a to c) Cryo-electron micrograph images of HPV16 capsids matured for 18 h (a), 4 h (b), and 1 h (c). (d) L1 C175S mutant capsids matured for 1 h. Note the presence of larger capsids in the 4-h and 1-h preparations. Larger capsids are indicated by asterisks. Bar (top left) = 200 Å.

forms of native virions of cottontail rabbit papillomavirus (11) (data not shown).

Figure 3 illustrates possible stages of condensation from a larger procapsid (Fig. 3e) to the mature capsid (Fig. 3a). There is a minor (~5%) diameter difference between the procapsids shown in panels e and a. However, the radius of the capsid was determined by calculating a 3D radial average, which does not account for the fact that there is an anisotropic contraction. The diameter at the 2-fold symmetry axis decreases by about 5%, the diameter at the 3-fold axis decreases by about 3%, and the diameter at the 5-fold axis decreases by about 12%. Figure 3, column 1, illustrates the 2-fold outside exterior view of successively larger capsids. In column 2, which illustrates an interior view of the capsid, decreasing connectedness between neighboring capsomers is clearly visible in the less mature capsid species. The third column of Fig. 3 shows the protein density (in black) at a radius of 260 Å for mature capsids (a) scaled by diameter for panels b to e. Note the presence of connections between capsomers at the top, which disappear as the capsid is observed in less mature states.

Finally, we analyzed capsids produced using HPV16 L1 carrying a Cys_{175}→Ser mutation (6), which prevents the formation of Cys_{175}-Cys_{428} disulfide bonds, which are essential for maturation. Although Cys_{175} is critically involved in the formation of inter-L1 disulfide cross-links, the C175S mutation does not abrogate infectivity *in vitro* (6). We anticipated that the structure of this mutant would be a larger procapsid. Analysis of 1,910 images obtained from 28 micrographs (Fig. 1d) yielded two size classes, where the first (smaller) class was 8% larger than mature wild-type (wt) capsids (Fig. 4a and c). The larger class (Fig. 4b and d) was similar in appearance to larger wt classes and 9% larger than wt mature capsids. A substantial number of even larger capsids were discernible in raw images, but attempted analyses of the larger classes converged to the two classes described above. Statistics for the

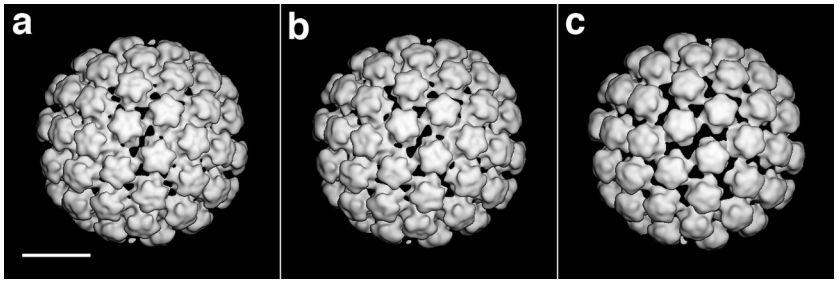

FIG 2 Computer analysis of the capsids allowed to mature for 18 h provided a 3D reconstruction of mature HPV16 capsids (a) as well as two slightly larger, presumably less mature capsids (b and c). All images have had their internal DNA computationally removed in order to visualize the protein capsid. The mature capsid (a) contained 1,026 images and has a nominal diameter of 600 Å. The next capsid class (b) contained 1,106 images and has a 610-Å diameter. The least mature capsid (c) contained 1,296 images and has a 626-Å diameter. Bar = 200 Å.

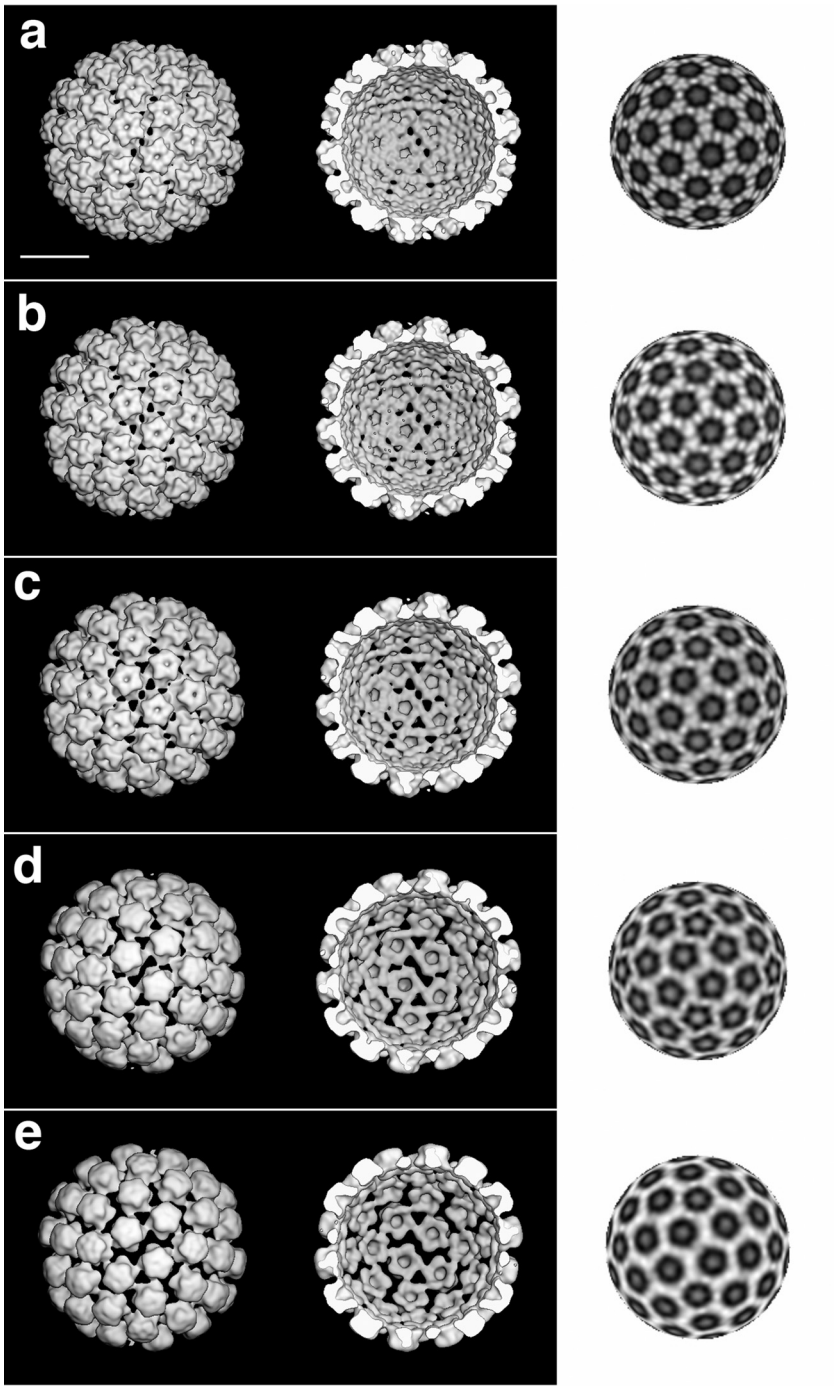

FIG 3 Combining 18-h, 4-h, and 1-h capsids provided a 3D reconstruction of mature 600 Å capsids (a) as well as four intermediates ranging in size from (nominally) a 605-Å diameter to a 633-Å diameter (b to e). All images have had their internal DNA computationally removed in order to visualize the protein capsid shell. The relative size and number of particles for each class are as follows: (a) 600 Å, 1,675 particles; (b) 607 Å, 591 particles; (c) 612 Å, 588 particles; (d) 619 Å, 982 particles; (e) 633 Å, 1,252 particles. The first column shows the 2-fold view. The second column shows the same view with the front half removed. The third column shows radial density at a radius of 260 Å (a) and scaled by diameter (b to e). Bar = 200 Å. The same results are presented as an animated file in Fig. S3 in the supplemental material.

maturation-incompetent mutant capsid preparation are shown in Table S2 in the supplemental material.

Improved maturation. A cryo-EM based study of bovine papillomavirus 1 (BPV1) virions (18) further refined a previously proposed model for the topology of the L1 "invading arms" that link together neighboring capsomer knobs (19). In both models, the capsid is stabilized by two types of inter-L1 disulfide bonds. Topologically ring-shaped L1 trimers surround each pentavalent (vertex) capsomer, while reciprocal L1 dimers extend between neighboring hexavalent capsomers. Although the model predicts a

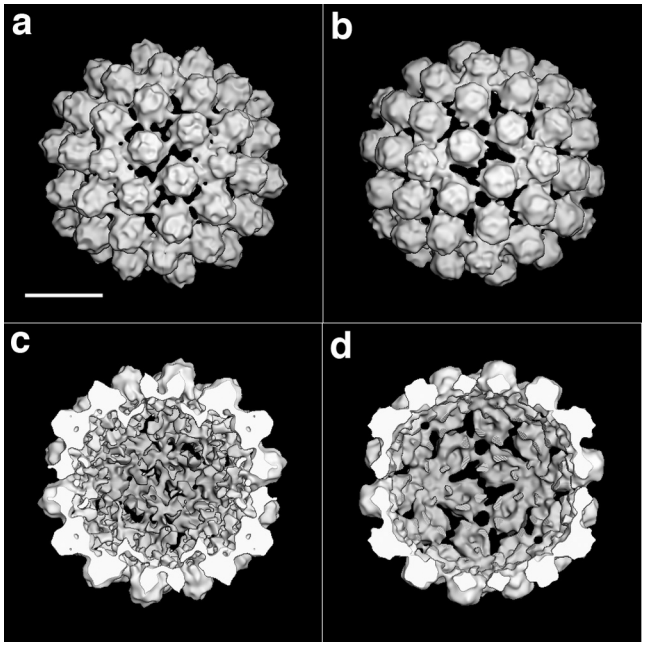

FIG 4 C175S mutant HPV16 capsids, which cannot form cystine 175 cross-links, provided the following final result starting from 3 wt models, a, d, and e (Fig. 3). Refinement converged into two models: smaller capsids (a) as well as larger, less mature capsids (b). There were 582 images in the smaller (a) and 771 images in the larger (b). Cutaway views of panels a and b are shown in panels c and d, respectively. Their respective resolutions are 34 Å and 29 Å (FSC = 0.3). Bar = 200 Å.

single species of L1 trimer and a single species of L1 dimer, a long-standing puzzle has been the appearance of two distinct species of disulfide-linked L1 trimer and two distinct species of L1 dimer in denaturing/nonreducing SDS-PAGE analyses of recombinant papillomavirus capsids (6, 19). Given our observation of low levels of less mature particles in capsid preparations allowed to mature for 18 h, we speculated that the additional L1 dimer and trimer bands might represent incomplete maturation. For example, failure to complete one disulfide bond in the proposed ring trimer would result in a linear trimer that might migrate differently in SDS-PAGE gels. Likewise, failure to form one of the disulfide bonds in the proposed reciprocal dimer would result in a topologically T-shaped dimer that might migrate differently in SDS-PAGE gels. A cartoon of this model is provided in reference 20 and on our lab website (http://home.ccr.cancer.gov/Lco/ImprovedMaturation.htm).

We hypothesized that formation of inter-L1 disulfide bonds during the maturation process might be mediated by disulfide shuffling reactions involving oxidized glutathione in the cell lysate. In this two-step mechanism, a free sulfhydryl group on L1 would first attack the S-S bond in an oxidized glutathione dimer. The L1 would thus become decorated with an S-S-bonded glutathione monomer. In the second step, a free sulfhydryl group on a neighboring L1 molecule would attack the L1-glutathione disulfide bond, ejecting a reduced glutathione monomer and forming an intermolecular L1-L1 disulfide bond. The initial step in disulfide shuffling reactions is ionization of a free sulfhydryl group (SH) to thiolate (S^-). The pK_a of this ionization is roughly 8.3 (depending on the local chemical environment of the SH group). Using pH test strips, we found that the pH of infected cell lysates ranged from 6.0 to 6.5. By adding buffering agents to the cell lysate, it was possible to stabilize the pH to roughly 8.0 immediately after cell lysis. The pH of the buffered lysate gradually fell to 7.0 by 18 h after cell lysis. Capsids allowed to mature in buffered lysate showed the expected one-dimer/one-trimer L1 cross-linking pattern in denaturing/nonreducing gels (Fig. 5). Analysis of native HPV2 virions extracted from human skin warts also showed the expected one-dimer/one-trimer pattern (see Fig. S2 in the supplemental material), confirming the idea that this pattern represents the completed ring trimer/reciprocal dimer maturation endpoint that predominates in virions matured through the natural process of keratinocyte differentiation.

Pseudoatomic model of the fully mature HPV16 capsid. Uniformly mature capsids produced in buffered cell lysate were sub-

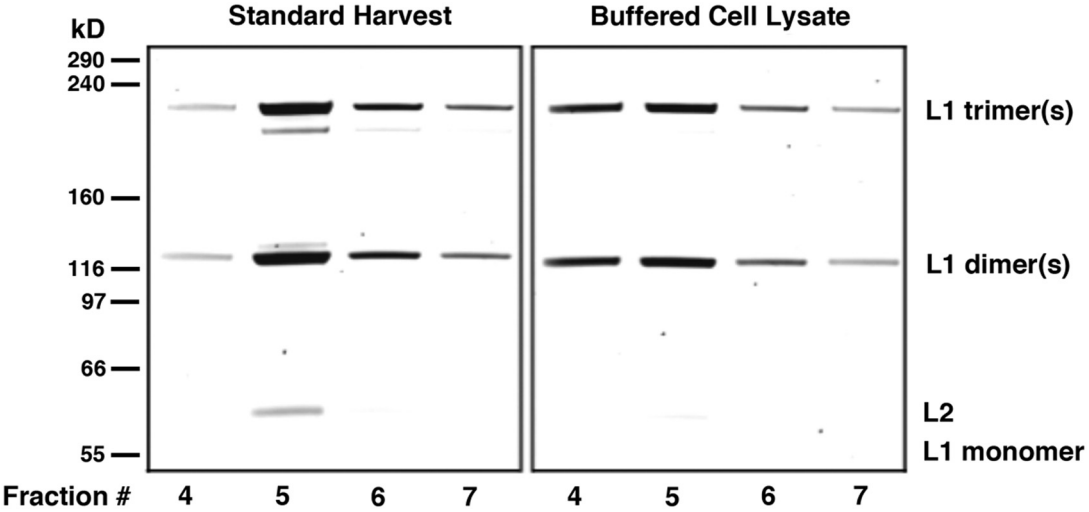

FIG 5 To facilitate the formation of intermolecular disulfide bonds between neighboring L1 molecules, lysates of 293TT cells expressing L1 were buffered with ammonium sulfate. Capsids derived from the buffered lysate exhibited a greater extent of maturation. This is reflected in a greater fraction of the slower-migrating ring trimer and faster-migrating reciprocal dimer.

jected to cryo-EM and digital image reconstruction. Using about 6,000 particles, we obtained a density map of the HPV16 capsid at 9.1-Å resolution (Fig. 6; also, see Fig. S4 in the supplemental material). At this resolution, secondary structure elements, such as α-helices, can be visually discriminated as rod-like densities, while other elements are only partially detectable. However, it is possible to derive an informative model of the structure by using flexible-fitting procedures, if a close atomic structure is available. In this case, the closest structure is the one previously obtained by crystallographic analysis of small (30-nm) T=1 virus-like particles (VLPs) assembled from an N- and C-truncated recombinant HPV16 L1 protein (21). A rigid-body fit of six separate copies of the X-ray crystal structure into the cryo-EM structure shows a good fit for the core of the capsomer knob (data not shown). The rigid-body fit includes two α-helices involving residues 386 to 402 and 463 to 472, which occupy the expected tubular densities.

The only major differences between the T=1 structure and the current cryo-EM structure are at the L1 N and C termini. Most notably, an α-helix involving residues 413 to 426 in the atomic model of the T=1 VLP is not apparent in the cryo-EM structure. In full-size virions, the C terminus of L1 is thought to form an elbow-shaped loop that extends into an adjacent capsomer and returns (18). In this model, the "invading" strand of the loop extends along the floor and up the walls of the canyons between capsomer knobs. The "elbow" at the apex of the loop forms an intercapsomeric disulfide bond involving HPV16 Cys175 and Cys428. The "returning" strand of the loop extends through the middle of the canyons to rejoin the donor capsomer. A lower-contrast density consistent with the returning strand of the loop is visible in the reconstructed map as a set of "suspended bridges" extending between the capsomer knobs. This can be seen in 3D radial density sections at the 264-Å radius (Fig. 6B).

Starting from the rigid fit, we sought to improve the model of the full-size T=7 capsid using flexible-fitting procedures. Before the fit, we removed the harmonic constraint for the absent 413-to-426 α-helix and added as many residues as the visual interpretation of the density allowed to both the N and C termini (residues 9 to 486). This approach resulted in arrangement of the C terminus of L1 into the expected elbow-shaped configuration, including the expected suspended bridge arrangement of the returning strand of the loop (Fig. 7; also, see Movie S1 in the supplemental material). As observed in the rigid fit, the knob-shaped cores of the six L1 chains remain equivalent and in agreement with the atomic model from the small T=1 VLP (root mean square difference [RMSD], ~1.1 Å). Movie S1 illustrates the finished pseudoatomic model of the capsid.

Comparison of our model of the full-size T=7 HPV16 capsid to the recent high-resolution cryo-EM-based model of BPV1 (18) reveals striking similarities, with L1 proteins organized in almost identical conformations, including the suspended-bridge configuration of the C terminus (Fig. 8). Importantly, the model for BPV1 shows that the N terminus of L1 extends toward adjacent capsomers to form a network of interpentameric contacts. Although we observed that the N terminus of HPV16 L1 extends toward the neighboring capsomer (as seen in the BPV1 capsid), our structure had insufficient resolution to confirm that the N-terminal nine residues ultimately contact the neighboring capsomer.

DISCUSSION

Three-dimensional reconstruction of time-lapse cryo-electron micrographs of HPV16 capsids reveals various conformations, likely representing intermediates in the transition from the immature procapsid to the fully mature capsid. The states demonstrate a regular progression of capsids shrinking from about 633 Å to 600 Å. However, it is likely that additional, larger states that cannot be resolved by 3D reconstructions also exist. The progressively smaller size of maturing capsids is consistent with the fact that maturation involves the increasing formation of disulfide cross-links between neighboring L1 capsid proteins.

The first analysis was performed on a capsid preparation allowed to mature for 18 h. Prior biochemical analysis (6) demonstrated that by 16 h there were extensive inter-L1 disulfide cross-links and few L1 monomers. In addition, capsids allowed to mature for 16 h were resistant to proteolysis by trypsin. In contrast, capsids allowed to mature for 4 h were susceptible to trypsin and had few inter-L1 disulfide cross-links. A structural study of what we believed were "mature" capsids at 18 h was done to verify that these capsids were identical to what one would expect from earlier analyses (22, 23). Careful examination of the cryo-electron micrographs indicated that there was an unexpected variation in capsid diameters (at least 5%). This variation led us to conclude that our "mature" specimen contained some fraction of less mature capsids. Computer analysis confirmed that there were three classes of capsids ranging in size from a normalized 600 Å (mature capsids, which were the most abundant capsid size) and two slightly larger classes (610 Å and 626 Å), suggesting that a fraction of capsids fail to achieve full maturation, even after 18 h. Therefore, our assumption that an 18-h preparation should contain only completely mature capsids was not entirely correct.

In an effort to visualize larger, less mature capsid species, we also performed analyses of capsids allowed to mature for 1 or 4 h (6). Although the less-mature-capsid preparations contained greater proportions of larger capsid species, a substantial portion of the capsid pool closely resembled capsids allowed to mature for 18 h. This result demonstrates that at least a fraction of capsids can achieve a regular, compact configuration even before the full complement of disulfide bonds have been formed. The structural analysis is consistent with the concept that HPV16 capsid maturation is a slow and asynchronous process.

We also performed structural studies on an L1 Cys_{175}→Ser mutant that does not mature (6). It was our expectation that we might be able to determine the structure of the procapsid in an early, larger icosahedral state that did not mature into (600-Å-diameter) capsids. Our analysis of the mutant capsids produced two interesting results. First, consistent with this mutant being infectious, it did form regular capsids, not unlike wt immature capsids. Second, the more mature (smaller) class was still significantly larger in diameter than wt mature capsids. It would appear from these results that the formation of a fully mature 600-Å capsid is dependent on the presence of cysteine 175 and that cross-link formation is an integral part of the shrinkage and formation of the final, fully mature state.

In cryo-electron micrographs of wild-type capsids, we observed a small fraction (~5%) of capsids at least 10 to 15% larger than any class that we were able to model. A histogram of the size distribution of capsids from the wt L1 1-h preparation indicates the presence of larger capsids with approximate diameters of 614,

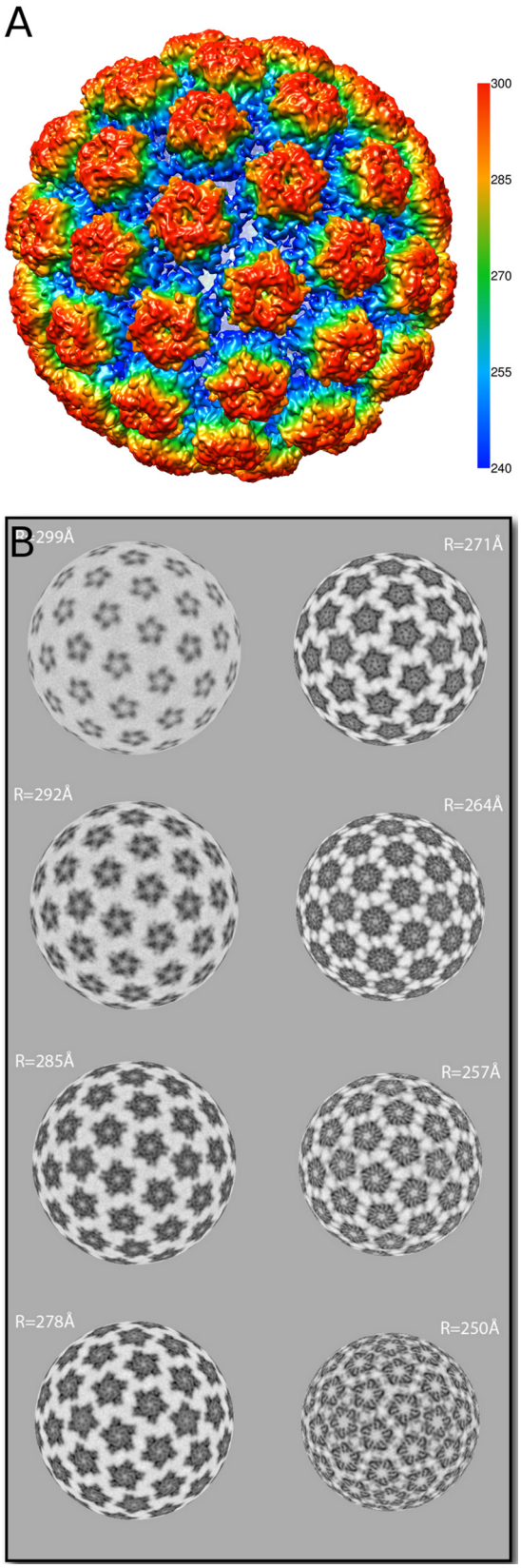

FIG 6 Reconstruction of a fully mature HPV16 capsid at 9 Å resolution. (A) Surface rendering of the capsid, colored according to radius. Radius values (color bar) are in angstroms. (B) Radial sections of the reconstruction taken at

(Continued)

634, and 650 Å (data not shown). That is, the histogram contained distinct peaks rather than a Gaussian trailing distribution of radii (data not shown). The peak at ~634 Å corresponds to our largest size class. None of these largest (~650-Å) capsids could be reconstructed. There are a few possible explanations. It could be that the largest procapsids do not follow strict icosahedral symmetry due to local deformation(s) or flattening. As a result, they cannot be combined into a 3D reconstruction using the icosahedral 3D reconstruction methods. Another possible explanation is that these large procapsids are a loose aggregate of major capsid proteins, but that they do not have the appropriate number (i.e., 72) of L1 capsomers. A third possibility is that we have too few examples of the larger procapsid class(es), such that we are unable to combine them into a 3D reconstruction. In any case, the cryo-electron micrographs clearly indicate the presence of larger procapsids, whose detailed structure could not be determined.

Although the largest reconstructible HPV16 capsid species appear to show holes in the capsid floor, it is important to note that immature capsids are closed tightly enough to exclude small nucleases (6). Thus, it is likely that loose protein connections between adjacent L1 molecules are present in immature capsids but are so disordered as to vanish in the reconstruction process.

During the maturation process, there is essentially no rotation of individual capsomers. The primary difference that arises during maturation is closure of the floor of the capsid, particularly in areas between hexavalent capsomers. More mature capsid species also exhibit a dimple on top of each capsomer. Band limiting the fully mature capsid reconstruction to the resolution of the largest capsid does not eliminate the dimple. We speculate that there are two possibilities. Either the less mature capsids do not contain a dimple, or there is less stability (e.g., because of high-temperature factors) at the outer radius of the less mature capsids.

Based on our initial cryo-EM results with capsids allowed to mature overnight and the appearance of minor amounts of unexpected L1 dimer and trimer species, we guessed that the maturation process remained incomplete in a fraction of capsids, even after overnight maturation. We found that buffering the cell lysate to a pH more compatible with disulfide shuffling reactions allows more uniform completion of the capsid maturation process.

The availability of more uniformly mature capsids allowed us to develop a higher-resolution structure of the mature capsid. This high-resolution structure allows us to assign the locations of the N- and C-terminal domains of L1 that knit together neighboring capsomers. Our results are consistent with a previous model for BPV1, in which a C-terminal portion of L1 (analogous to HPV16 residues 430 to 444) extends through the canyons between capsomer knobs as a suspended bridge. Interestingly, the epitope recognized by one well-studied HPV16-neutralizing antibody, H16.U4, maps to the residues that form the suspended bridge (24, 25). H16.U4 has previously been shown to disrupt interactions between mature HPV16 pseudovirions and heparan sulfate attachment receptors (26, 27), suggesting a possible role for the suspended bridge in attachment of the virus to the surface of cul-

Figure Legend Continued

7-Å increments. Shown are radii from 299 Å (near the tip of the capsomers) to 250 Å (close to the floor of the canyons between capsomers). An image taken from one electron micrograph of fully mature HPV16 capsids is shown in Fig. S4.

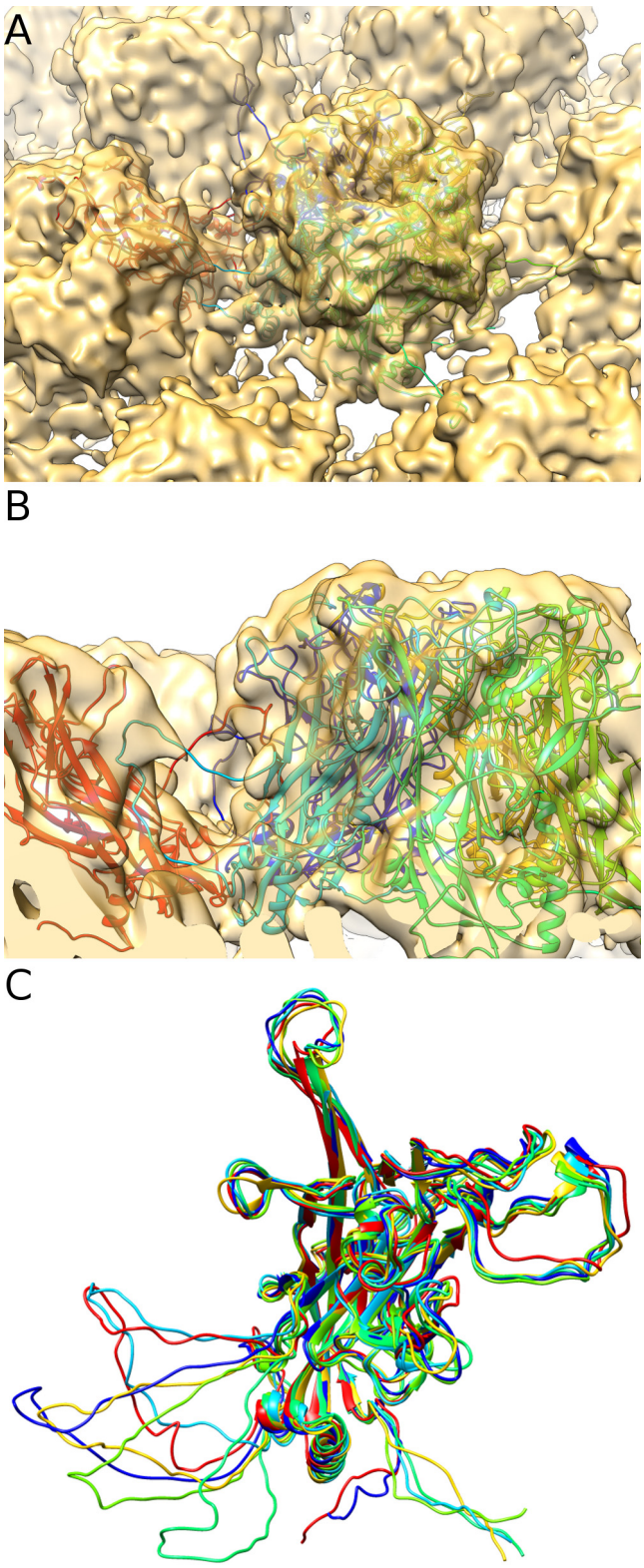

FIG 7 Pseudoatomic modeling of the mature HPV16 capsid. (A and B) Two views of the surface rendering of the capsid, shown in semitransparency, overlapped with the models obtained for the six subunits in one asymmetric unit, with each chain colored differently. The models were obtained by molecular dynamics-based flexible fitting, using the atomic coordinates available for the core of the HPV16 major capsid protein L1 (PDB ID, 1DZL) as a starting

(Continued)

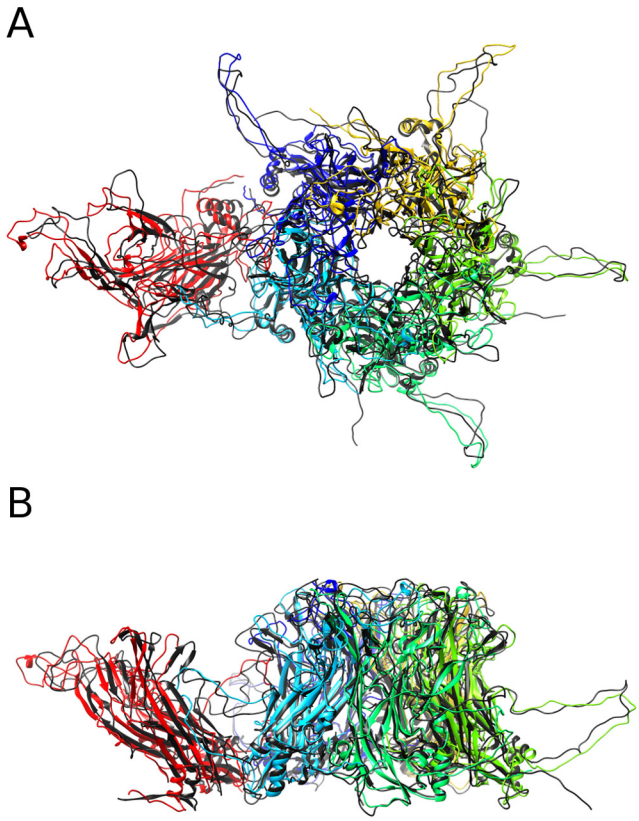

FIG 8 Comparison between models of HPV16 and BPV1. The model of BPV1 is from a cryo-EM reconstruction obtained by Wolf et al. (18) (PDB ID, 3IYJ). (A) Top view. (B) Side view. All the subunits of the BPV model are in black, while those of HPV16 are colored using the same scheme as in Fig. 7.

tured cells or to the epidermal basement membrane during infection *in vivo* (reviewed in reference 28). Enzyme-linked immunosorbent assay (ELISA) results have suggested that the H16.U4 target epitope is heterogeneously exposed on the surface of the virion and the MAb fails to efficiently recognize HPV16 pseudovirions that are bound to the cell surface (26). The idea that the suspended bridge is poorly accessible on the mature virion is also consistent with the observation that Arg437 (within the bridge) becomes resistant to cleavage with trypsin after pseudovirion maturation (6, 29). It would be interesting to know whether peptide immunogens based on the suspended bridge might elicit functionally neutralizing antibody responses.

It remains uncertain how the viral genome and L2 escape the L1 "cage" during the infectious entry process. It seems possible that disulfide shuffling events (perhaps mediated by protein disulfide isomerases or other chaperones) or chemical reduction of disulfide bonds might remove the inter-L1 cross-links that stabilize the mature virion. Although our observations show that L1 multimers can spontaneously collapse to monomers under nonreducing conditions in the presence of dodecyl sulfate or

Figure Legend Continued

reference. (C) Superposition of the six models obtained for the six nonequivalent locations of the protein L1 in one asymmetric unit. The differences between the models are only in the arrangement of the intercapsomeric connections formed by the N and C termini.

≥5 M urea (presumably due to disulfide shuffling), an extensive series of experiments did not reveal any accumulation of L1 monomers after application of pseudovirions to cultured cells. It may be that the HPV infectious entry process is too asynchronous to allow observation of L1 monomers at any given moment. Another possible explanation is that release of the viral genome does not involve the breaking or rearrangement of inter-L1 disulfide bonds and may instead depend on proteolytic cleavage of L1 or large-scale rearrangement of intercapsomeric contacts.

In herpes simplex virus type 1 (HSV-1), the procapsid consists of very loosely associated capsid proteins that form a continuous floor region during maturation, but with no net reduction in capsid diameter (30). Unlike HPV16, HSV-1 maturation also involves rotation and regularization of hexavalent capsomers. In addition, the diameter of the HSV-1 expands slightly and then shrinks during maturation, which contrasts with the shrinkage of the HPV16 capsid during maturation.

HK97, a bacteriophage, shows extensive rearrangement of major capsid proteins within each hexavalent capsomer, as well as a large expansion of the capsid during its maturation process (31). This type of maturational rearrangement is common in bacteriophages. In the case of HK97, the mature capsid is stabilized in a chainmail-style pattern of interlocking rings formed by isopeptide linkages among the capsomers (32). It has recently been proposed that the formation of these isopeptide linkages may serve to progressively fix in place increasingly mature conformations that arise spontaneously due to Brownian motion (33). This concept, referred to as a Brownian ratchet, might also be applied to the maturation of the papillomavirus capsid. In this model, an initial dynamic equilibrium of capsid states could be stabilized by the progressive formation of inter-L1 disulfide bonds, ultimately entrapping the capsid in increasingly mature configurations. Based on this assumption we have assembled an animated file showing the maturation progression to help visualize the closing up and shrinkage of the capsid shell (see Fig. S3 in the supplemental material).

MATERIALS AND METHODS

Pseudovirion production. HPV16 L1/L2 capsids were produced in mammalian 293TT cells as previously described (12). Briefly, an L1/L2 expression plasmid, p16L1L2, that is capable of high-yield self-packaging was used to produce a viral seed stock. A mutant version of the plasmid, p16mL1L2, carries a Cys_{175}→Ser mutation in L1 (6). Since freezing diminished the titer of the p16mL1L2 seed stock, it was prepared fresh immediately prior to use. To produce capsids, 1.5×10^7 293TT cells were preplated overnight in a 225-cm^2 flask and then infected with 30 μl of p16L1L2 seed stock or 60 μl of p16mL1L2 seed stock. After 72 h, infected cells were lysed at high density (10^8 cells/ml) in Dulbecco's PBS (DPBS) with 0.5% Brij 58 and a nuclease cocktail. The resulting Brij lysates of infected cells were incubated at 37°C for 1, 4, or 18 h to allow various degrees of maturation. Cys_{175}→Ser mutant capsids were allowed to mature for 1 h. The lysates were chilled, adjusted to 0.85 M NaCl, and incubated on ice for 10 min. Lysates were then clarified by centrifugation at 10,000 × *g* for 10 min.

For endpoint maturation of pseudovirions, cells were lysed using 0.5% Triton X-100 instead of Brij 58, and the cell lysate was adjusted to 25 mM ammonium sulfate using a 1 M ammonium sulfate stock adjusted to pH 9.0. In separate experiments, Tris base at a final concentration of 10 mM or 40 mM $NaPO_4$ (starting from a 1 M stock, pH 7.5) were both roughly as effective as ammonium sulfate for promoting complete capsid maturation (data not shown).

Detailed protocols for capsid production are available from *Current Protocols in Cell Biology* (34) and on our laboratory website (http://home.ccr.cancer.gov/LCO/).

Pseudovirion and virion purification. Capsids were purified from clarified cell lysate using agarose gel filtration columns. Non-cross-linked agarose beads (2%; Agarose Bead Technologies) were poured into 2-ml polystyrene columns (Pierce). The columns were blocked overnight with 1% BSA in DPBS with a total of 500 mM NaCl (DPBS/0.5). Prior to use, the columns were washed with DPBS/0.5 supplemented with 0.01% Brij 58. Eluted fractions were screened using a bicinchoninic acid (BCA) protein assay kit (Pierce). L1 yield and purity were also assessed by Coomassie staining (Protiga) of NuPAGE gels (Invitrogen) or by Western blotting using the antibody CamVir-1 (Pharmingen), as previously described (6).

Native HPV virions were purified from human skin warts that had been discarded after surgical excision for therapeutic reasons. All specimens were anonymized. Warts were minced with a blade 10 scalpel in 0.5 ml of DPBS with 10 mM $MgCl_2$ and 1% Brij 58 in a 6-cm petri dish. The suspended minced material was transferred to a 1.5-ml siliconized tube. Two microliters each of Benzonase (Sigma) and Plasmid-Safe (Epicentre) were added, and the mixture was incubated for 20 min at 37°C. Roughly 5 mg of collagenase (Sigma C8051) was added, and the mixture was incubated for an additional 30 min at 37°C. NaCl was added to a final concentration of roughly 1 M, and the mixture was incubated overnight at 4°C. The suspension was clarified for 5 min at 5,000 × *g*, and a first supernatant was collected. The pelleted material was resuspended in 0.5 ml of DPBS with 0.8 M NaCl and sonicated three times for 1 min in a Misonix cup sonicator. The sample was reclarified, and the first and second supernatants were pooled, reclarified, and applied to a 27-33-39% Optiprep gradient as previously described (17, 34).

Nonreducing denaturing gel analysis. Virion or pseudovirion preparations were alkylated using *N*-ethyl maleimide (NEM; Pierce). Iodoacetamide was dramatically less effective than NEM for preventing collapse into monomers, presumably due to SDS inhibition of iodoacetamide's alkylating capacity (35). Alkylation was conducted by diluting roughly 1 μg of L1 into 10 mM $NaPO_4$ (pH 6.5) and then adding 10 mM NEM for 10 min at room temperature. A 3× stock of neutral load dye was used to adjust the sample to a final concentration of 2% lithium dodecyl sulfate (LDS), 100 mM Tris (pH 6.8), 10 mM NEM, 5 mM EDTA, 10% glycerol, and 0.01% bromophenol blue. In some instances, NuPage LDS sample buffer (Invitrogen) supplemented with 10 mM NEM was used with results similar to the neutral load dye. The 1× load dye sample was incubated at room temperature for 10 min and then at 65°C for 10 min. The alkylated sample was run on 3 to 8% NuPage Tris-acetate gels (Invitrogen). Gels were stained using SYPRO Ruby stain (Invitrogen) and imaged on an LAS4000 (Fuji). Band size was estimated by comparison to a HiMark unstained protein ladder (Invitrogen).

Analysis of cryo-electron microscopic images. Cryo-electron micrographs were taken on a CM200-FEG electron microscope (FEI, Mahwah, NJ) at a magnification of ×38,000. Micrographs were recorded at defocus settings such that the first contrast transfer function zeros were at frequencies of 1/16 $Å^{-1}$ to 1/20 $Å^{-1}$. Micrographs were digitized on an SCAI scanner (Z/I Imaging, Huntsville, AL) at 7 μm/pixel and binned to give 14-μm pixels (3.71 Å at the specimen). Particles were extracted and preprocessed using the graphical program X3D (36). Initial estimates of the orientation angles were determined by with the polar Fourier transform (PFT) algorithm (37), using a BPV1 structure (23) as a starting model that was scaled to match the current data. Initial analyses were performed on three sets of data, which were allowed to mature for 1, 4, and 18 h after cell lysis. Once a low-resolution 3D HPV16 reconstruction was obtained that was distinctly papillomavirus-like, it was used as a model for subsequent refinement. Cys_{175}→Ser mutant capsids were analyzed as described above. Micrographs of fully mature pseudovirions were taken at a higher magnification (×50,000) corresponding to 1.41 Å at the specimen and processed as described above. A more detailed explanation of model searching, refinement, and classification is diagrammed in Fig. S1 in the supplemental material. A total of 8,651 particles were extracted from the

20 micrographs acquired, but only 5,952 particles were used for the final reconstruction. The resolution was assessed by calculating the Fourier shell correlation (FSC) curve between the maps from two half-sets and measuring the spatial frequency at which the curve fell below 0.5. Before the FSC calculation, a soft mask was applied to the maps to keep only the density features in the radial zone between 196 Å and 323 Å.

Consistent with previous work (6), a substantial majority of pseudovirions were observed to contain DNA. Based on previous analytical analysis of full capsids produced similarly, we expect the average occupancy to be close to 100%.

Pseudoatomic modeling of the fully mature HPV16 capsid. The atomic model of a truncated HPV16 L1 VLP (PDB ID, 1DZL; residues 20 to 474) (21) was manually fitted into the density of the cryo-EM reconstruction of fully mature HPV16 using the tool Fit In Map in Chimera (38). Copies of the model were placed in all six subunits, forming one asymmetric unit. The model was then extended at both the N and C termini to include missing residues in the X-ray model, until they could be uniquely assigned to density in the reconstruction. Specifically, 11 residues at the N terminus and 12 residues at the C terminus were modeled as random-coil segments (final residues 9 to 486). The coordinates of the additional residues and the C-terminal arm looping out from the subunit core were adjusted to agree with the density visible in the reconstruction using the "sculpting" tool in PyMOL (39). The constraints on the helix present in the original model in the C-terminal arm were removed, because no rod-like density could be observed in the reconstruction at the corresponding location. Energy minimization using visual molecular dynamics (VMD) (40) was then performed on the full asymmetric unit to relax steric clashes between the six models. Finally, the complete atomic model of one asymmetric unit was refined using molecular dynamic flexible fitting (MDFF) (41). For this task, we developed a specific protocol that incorporates the symmetry constraints of the virus without the need to model the full capsid. The procedure is iterative and combines tools from NAMD molecular dynamics software (42), Chimera, and Bsoft (43). At each iteration, the current solution for the model, in combination with copies of the five closest neighboring asymmetric units, was used to segment the corresponding density map in the reconstruction (tools Sym, Color Zone, and Split Map in Chimera). The resulting subvolume was filtered to the nominal resolution of the reconstruction to smooth the edges of the cropped density. Then, a molecular dynamics simulation of 50 ps was run *in vacuo* using MDFF in NAMD, where the secondary structure of the model is restrained and the filtered density provides an additional force field. This procedure was repeated for 8 iterations. Finally, the boundaries of the model were refined by performing 2,000 iterations of energy minimization on a composite model containing the latest solution and copies of the 5 neighboring units, including the corresponding density as an additional force field. The difference between the L1 models obtained from this procedure and both the models from the truncated HPV16 L1 VLP (PDB ID, 1DZL) and those from the high-resolution BPV1 cryo-EM reconstruction (PDB ID, 3IYJ) (18) were measured as root mean square deviations (RMSD) using the tool Matchmaker in Chimera. A pseudoatomic model that includes possible arrangements of amino acid side chains is posted on our lab website (http://home.ccr.cancer.gov/Lco/L1structure.asp).

Data bank accession number. A cryo-EM map of the fully mature capsid was deposited in EMDataBank (accession no. EMD-5932). Coordinates for the pseudoatomic model of the peptide backbone were deposited in PDB (accession no. 3J6R).

SUPPLEMENTAL MATERIAL

Supplemental material for this article may be found at http://mbio.asm.org/lookup/suppl/doi:10.1128/mBio.01104-14/-/DCSupplemental.

Text S1, PDF file, 0.1 MB.
Figure S1, TIFF file, 1.5 MB.
Figure S2, TIFF file, 1.5 MB.
Figure S3, PPTX file, 0.8 MB.
Figure S4, TIFF file, 1.5 MB.
Table S1, PDF file, 0.1 MB.
Table S2, PDF file, 0.1 MB.
Movie S1, MOV file, 13.9 MB.

ACKNOWLEDGMENTS

This research was supported in part by the Intramural Research Program of the NIH, the Center for Information Technology (CIT) the National Cancer Institute's Center for Cancer Research, and the National Institute of Arthritis, Musculoskeletal and Skin Diseases. Part of the molecular graphics and analyses were performed with the UCSF Chimera package. Chimera is developed by the Resource for Biocomputing, Visualization, and Informatics at the University of California San Francisco (supported by NIGMS P41-GM103311).

We are pleased to acknowledge T. Baker, D. Belnap, J. Conway, and J. B. Heymann for software and programming contributions.

REFERENCES

1. **Jabłońska S, Majewski S, Obalek S, Orth G.** 1997. Cutaneous warts. Clin. Dermatol. **15:**309–319. http://dx.doi.org/10.1016/S0738-081X(96)00170-8.
2. **Schiffman M, Kjaer SK.** 2003. Chapter 2: natural history of anogenital human papillomavirus infection and neoplasia. J. Natl. Cancer Inst. Monogr. **31:**14–19.
3. **Arbyn M, de Sanjosé S, Saraiya M, Sideri M, Palefsky J, Lacey C, Gillison M, Bruni L, Ronco G, Wentzensen N, Brotherton J, Qiao YL, Denny L, Bornstein J, Abramowitz L, Giuliano A, Tommasino M, Monsonego J.** 2012. EUROGIN 2011 roadmap on prevention and treatment of HPV-related disease. Int. J. Cancer **131:**1969–1982. http://dx.doi.org/10.1002/ijc.27650.
4. **Doorbar J.** 2005. The papillomavirus life cycle. J. Clin. Virol. **32**(Suppl 1):S7–S15. http://dx.doi.org/10.1016/j.jcv.2004.04.002.
5. **Holmgren SC, Patterson NA, Ozbun MA, Lambert PF.** 2005. The minor capsid protein L2 contributes to two steps in the human papillomavirus type 31 life cycle. J. Virol. **79:**3938–3948. http://dx.doi.org/10.1128/JVI.79.7.3938-3948.2005.
6. **Buck CB, Thompson CD, Pang YY, Lowy DR, Schiller JT.** 2005. Maturation of papillomavirus capsids. J. Virol. **79:**2839–2846. http://dx.doi.org/10.1128/JVI.79.5.2839-2846.2005.
7. **Sapp M, Volpers C, Müller M, Streeck RE.** 1995. Organization of the major and minor capsid proteins in human papillomavirus type 33 virus-like particles. J. Gen. Virol. **76:**2407–2412. http://dx.doi.org/10.1099/0022-1317-76-9-2407.
8. **Li M, Beard P, Estes PA, Lyon MK, Garcea RL.** 1998. Intercapsomeric disulfide bonds in papillomavirus assembly and disassembly. J. Virol. **72:**2160–2167.
9. **Sapp M, Fligge C, Petzak I, Harris JR, Streeck RE.** 1998. Papillomavirus assembly requires trimerization of the major capsid protein by disulfides between two highly conserved cysteines. J. Virol. **72:**6186–6189.
10. **Steven AC, Heymann JB, Cheng N, Trus BL, Conway JF.** 2005. Virus maturation: dynamics and mechanism of a stabilizing structural transition that leads to infectivity. Curr. Opin. Struct. Biol. **15:**227–236. http://dx.doi.org/10.1016/j.sbi.2005.03.008.
11. **Belnap DM, Olson NH, Cladel NM, Newcomb WW, Brown JC, Kreider JW, Christensen ND, Baker TS.** 1996. Conserved features in papillomavirus and polyomavirus capsids. J. Mol. Biol. **259:**249–263. http://dx.doi.org/10.1006/jmbi.1996.0317.
12. **Buck CB, Cheng N, Thompson CD, Lowy DR, Steven AC, Schiller JT, Trus BL.** 2008. Arrangement of L2 within the papillomavirus capsid. J. Virol. **82:**5190–5197. http://dx.doi.org/10.1128/JVI.02726-07.
13. **Hagel L.** 2001. Gel-filtration chromatography. Curr. Protoc. Protein Sci. Chapter **8:**Unit 83. http://dx.doi.org/10.1002/0471140864.ps0803s14.
14. **Buck CB, Pastrana DV, Lowy DR, Schiller JT.** 2005. Generation of HPV pseudovirions using transfection and their use in neutralization assays. Methods Mol. Med. **119:**445–462. http://dx.doi.org/10.1385/1-59259-982-6:445.
15. **Zhao Q, Wu S, Manger W, Gadam S.** August 2002. Process for making human papillomavirus virus-like particles with improved properties. U.S. patent 6,436,402.
16. **Shi L, Sanyal G, Ni A, Luo Z, Doshna S, Wang B, Graham TL, Wang N, Volkin DB.** 2005. Stabilization of human papillomavirus virus-like par-

ticles by non-ionic surfactants. J. Pharm. Sci. **94:**1538–1551. http://dx.doi.org/10.1002/jps.20377.
17. **Buck CB, Pastrana DV, Lowy DR, Schiller JT.** 2004. Efficient intracellular assembly of papillomaviral vectors. J. Virol. **78:**751–757. http://dx.doi.org/10.1128/JVI.78.2.751-757.2004.
18. **Wolf M, Garcea RL, Grigorieff N, Harrison SC.** 2010. Subunit interactions in bovine papillomavirus. Proc. Natl. Acad. Sci. USA **107:**6298–6303. http://dx.doi.org/10.1073/pnas.0914604107.
19. **Modis Y, Trus BL, Harrison SC.** 2002. Atomic model of the papillomavirus capsid. EMBO J. **21:**4754–4762. http://dx.doi.org/10.1093/emboj/cdf494.
20. **Buck CB, Trus BL.** 2012. The papillomavirus virion: a machine built to hide molecular Achilles' heels, p 403–422. *In* Rossmann MG, Rao VB (ed), Viral molecular machines, vol. **XIV**. Springer Verlag, Berlin, Germany.
21. **Chen XS, Garcea RL, Goldberg I, Casini G, Harrison SC.** 2000. Structure of small virus-like particles assembled from the L1 protein of human papillomavirus 16. Mol. Cell **5:**557–567. http://dx.doi.org/10.1016/S1097-2765(00)80449-9.
22. **Hagensee ME, Yaegashi N, Galloway DA.** 1993. Self-assembly of human papillomavirus type 1 capsids by expression of the L1 protein alone or by coexpression of the L1 and L2 capsid proteins. J. Virol. **67:**315–322.
23. **Trus BL, Roden RB, Greenstone HL, Vrhel M, Schiller JT, Booy FP.** 1997. Novel structural features of bovine papillomavirus capsid revealed by a three-dimensional reconstruction to 9-A resolution. Nat. Struct. Biol. **4:**413–420. http://dx.doi.org/10.1038/nsb0597-413.
24. **Roden RB, Armstrong A, Haderer P, Christensen ND, Hubbert NL, Lowy DR, Schiller JT, Kirnbauer R.** 1997. Characterization of a human papillomavirus type 16 variant-dependent neutralizing epitope. J. Virol. **71:**6247–6252.
25. **Carter JJ, Wipf GC, Benki SF, Christensen ND, Galloway DA.** 2003. Identification of a human papillomavirus type 16-specific epitope on the C-terminal arm of the major capsid protein L1. J. Virol. **77:**11625–11632. http://dx.doi.org/10.1128/JVI.77.21.11625-11632.2003.
26. **Day PM, Thompson CD, Buck CB, Pang YY, Lowy DR, Schiller JT.** 2007. Neutralization of human papillomavirus with monoclonal antibodies reveals different mechanisms of inhibition. J. Virol. **81:**8784–8792. http://dx.doi.org/10.1128/JVI.00552-07.
27. **Day PM, Gambhira R, Roden RB, Lowy DR, Schiller JT.** 2008. Mechanisms of human papillomavirus type 16 neutralization by L2 cross-neutralizing and L1 type-specific antibodies. J. Virol. **82:**4638–4646. http://dx.doi.org/10.1128/JVI.00143-08.
28. **Schiller JT, Day PM, Kines RC.** 2010. Current understanding of the mechanism of HPV infection. Gynecol. Oncol. **118:**S12–S17. http://dx.doi.org/10.1016/j.ygyno.2010.04.004.
29. **Chen XS, Casini G, Harrison SC, Garcea RL.** 2001. Papillomavirus capsid protein expression in Escherichia coli: purification and assembly of HPV11 and HPV16 L1. J. Mol. Biol. **307:**173–182. http://dx.doi.org/10.1006/jmbi.2000.4464.
30. **Heymann JB, Cheng N, Newcomb WW, Trus BL, Brown JC, Steven AC.** 2003. Dynamics of herpes simplex virus capsid maturation visualized by time-lapse cryo-electron microscopy. Nat. Struct. Biol. **10:**334–341. http://dx.doi.org/10.1038/nsb922.
31. **Conway JF, Wikoff WR, Cheng N, Duda RL, Hendrix RW, Johnson JE, Steven AC.** 2001. Virus maturation involving large subunit rotations and local refolding. Science **292:**744–748. http://dx.doi.org/10.1126/science.1058069.
32. **Duda RL.** 1998. Protein chain mail: catenated protein in viral capsids. Cell **94:**55–60. http://dx.doi.org/10.1016/S0092-8674(00)81221-0.
33. **Ross PD, Cheng N, Conway JF, Firek BA, Hendrix RW, Duda RL, Steven AC.** 2005. Crosslinking renders bacteriophage HK97 capsid maturation irreversible and effects an essential stabilization. EMBO J. **24:**1352–1363. http://dx.doi.org/10.1038/sj.emboj.7600613.
34. **Buck CB, Thompson CD.** 2007. Production of papillomavirus-based gene transfer vectors. Curr. Protoc. Cell Biol. Chapter 26:Unit 26.21. http://dx.doi.org/10.1002/0471143030.cb2601s37.
35. **Galvani M, Hamdan M, Herbert B, Righetti PG.** 2001. Alkylation kinetics of proteins in preparation for two-dimensional maps: a matrix assisted laser desorption/ionization-mass spectrometry investigation. Electrophoresis **22:**2058–2065. http://dx.doi.org/10.1002/1522-2683(200106)22:10<2058::AID-ELPS2058>3.0.CO;2-Z.
36. **Conway JF, Trus BL, Booy FP, Newcomb WW, Brown JC, Steven AC.** 1993. The effects of radiation damage on the structure of frozen hydrated HSV-1 capsids. J. Struct. Biol. **111:**222–233. http://dx.doi.org/10.1006/jsbi.1993.1052.
37. **Baker TS, Cheng RH.** 1996. A model-based approach for determining orientations of biological macromolecules imaged by cryoelectron microscopy. J. Struct. Biol. **116:**120–130. http://dx.doi.org/10.1006/jsbi.1996.0020.
38. **Pettersen EF, Goddard TD, Huang CC, Couch GS, Greenblatt DM, Meng EC, Ferrin TE.** 2004. UCSF Chimera—a visualization system for exploratory research and analysis. J. Comput. Chem. **25:**1605–1612. http://dx.doi.org/10.1002/jcc.20084.
39. **Schrodinger LLC.** 2010. The PyMOL molecular graphics system, version 1.3r1. Schrodinger LLC, Portland, OR.
40. **Humphrey W, Dalke A, Schulten K.** 1996. VMD: visual molecular dynamics. J. Mol. Graph. **14:**33–38. http://dx.doi.org/10.1016/0263-7855(96)0018-5.
41. **Trabuco LG, Villa E, Mitra K, Frank J, Schulten K.** 2008. Flexible fitting of atomic structures into electron microscopy maps using molecular dynamics. Structure **16:**673–683. http://dx.doi.org/10.1016/j.str.2008.03.005.
42. **Phillips JC, Braun R, Wang W, Gumbart J, Tajkhorshid E, Villa E, Chipot C, Skeel RD, Kalé L, Schulten K.** 2005. Scalable molecular dynamics with NAMD. J. Comput. Chem. **26:**1781–1802. http://dx.doi.org/10.1002/jcc.20289.
43. **Heymann JB, Cardone G, Winkler DC, Steven AC.** 2008. Computational resources for cryo-electron tomography in Bsoft. J. Struct. Biol. **161:**232–242. http://dx.doi.org/10.1016/j.jsb.2007.08.002.